



Silicon-Based Quantum Plasmonics for Chip-Integrated Single and Few Photon Information Systems

**Harry Atwater
CALIFORNIA INSTITUTE OF TECHNOLOGY**

**03/07/2019
Final Report**

DISTRIBUTION A: Distribution approved for public release.

**Air Force Research Laboratory
AF Office Of Scientific Research (AFOSR)/ RTB1
Arlington, Virginia 22203
Air Force Materiel Command**

DISTRIBUTION A: Distribution approved for public release.

REPORT DOCUMENTATION PAGE				<i>Form Approved</i> OMB No. 0704-0188	
<p>The public reporting burden for this collection of information is estimated to average 1 hour per response, including the time for reviewing instructions, searching existing data sources, gathering and maintaining the data needed, and completing and reviewing the collection of information. Send comments regarding this burden estimate or any other aspect of this collection of information, including suggestions for reducing the burden, to Department of Defense, Executive Services, Directorate (0704-0188). Respondents should be aware that notwithstanding any other provision of law, no person shall be subject to any penalty for failing to comply with a collection of information if it does not display a currently valid OMB control number.</p> <p>PLEASE DO NOT RETURN YOUR FORM TO THE ABOVE ORGANIZATION.</p>					
1. REPORT DATE (DD-MM-YYYY) 08-11-2019		2. REPORT TYPE Final Performance		3. DATES COVERED (From - To) 01 Nov 2015 to 31 Oct 2018	
4. TITLE AND SUBTITLE Silicon-Based Quantum Plasmonics for Chip-Integrated Single and Few Photon Information Systems				5a. CONTRACT NUMBER	
				5b. GRANT NUMBER FA9550-16-1-0019	
				5c. PROGRAM ELEMENT NUMBER 61102F	
6. AUTHOR(S) Harry Atwater				5d. PROJECT NUMBER	
				5e. TASK NUMBER	
				5f. WORK UNIT NUMBER	
7. PERFORMING ORGANIZATION NAME(S) AND ADDRESS(ES) CALIFORNIA INSTITUTE OF TECHNOLOGY 1200 E. CALIFORNIA BLDV PASADENA, CA 91125 US				8. PERFORMING ORGANIZATION REPORT NUMBER	
9. SPONSORING/MONITORING AGENCY NAME(S) AND ADDRESS(ES) AF Office of Scientific Research 875 N. Randolph St. Room 3112 Arlington, VA 22203				10. SPONSOR/MONITOR'S ACRONYM(S) AFRL/AFOSR RTB1	
				11. SPONSOR/MONITOR'S REPORT NUMBER(S) AFRL-AFOSR-VA-TR-2019-0334	
12. DISTRIBUTION/AVAILABILITY STATEMENT A DISTRIBUTION UNLIMITED: PB Public Release					
13. SUPPLEMENTARY NOTES					
14. ABSTRACT Under this grant the properties of quantum emitters suitable for silicon-based platforms were explored. During the grant period 2015-2018, we made advances in three main thematic areas: i) entanglement of surface plasmons under conditions of extreme plasmonic dispersion, ii) control of single-emitter position and local density of states, iii) spontaneous parametric downconversion.					
15. SUBJECT TERMS Few Photon Information Systems, plasmonics, Quantum Plasmonics, quantum coherence, nanophotonics, single photon					
16. SECURITY CLASSIFICATION OF:			17. LIMITATION OF ABSTRACT UU	18. NUMBER OF PAGES	19a. NAME OF RESPONSIBLE PERSON POMRENKE, GERNOT
a. REPORT Unclassified	b. ABSTRACT Unclassified	c. THIS PAGE Unclassified			19b. TELEPHONE NUMBER (Include area code) 703-696-8426

Final Performance Report for “Silicon-Based Quantum Plasmonics for Chip-Integrated Single and Few Photon Information Systems”

Air Force Office of Scientific Research Grant FA9550-16-1-0019

P.I. Harry A. Atwater

Summary

Under this grant the properties of quantum emitters suitable for silicon-based platforms were explored. During the grant period 2015-2018, we made advances in three main thematic areas:

- i) Entanglement of surface plasmons under conditions of extreme plasmonic dispersion
- ii) Control of single-emitter position and local density of states
- iii) Spontaneous parametric downconversion.

The entanglement effort built upon our earlier work on two-plasmon quantum interference (Fakonas, et.al., Nature Photonics, 2014), which was performed using plasmonic waveguides with modest dispersion. In this project we found, using a polarization entanglement scheme, that even for excitation near their surface plasmon resonance that exhibit extreme dispersion, there was no decrease in visibility of entanglement, strongly suggesting that highly dispersive plasmon excitation does not lead to plasmon dephasing.

In 2017, we began a second effort to exploit our previous “plasMOStor” field effect plasmonic modulator configuration to modify the local density of states (LDOS) near quantum emitters, specifically CdSe quantum dots. Gated plasmonic heterostructures used to deplete or accumulate carriers in titanium nitride were found to tune the LDOS and variously increase or decrease the spontaneous emission rate and radiative quantum efficiency, under gated electrical bias control. This essentially represents a new way to electrically modulate light output from an emitter, not by injecting a greater current density, but by changing the LDOS at constant injection rate by optical pumping.

A third main effort in this program was to develop a general theory for the physics of spontaneous parametric downconversion in ‘special’ media such as waveguides or hyperbolic metamaterials. Together, these efforts have resulted in advances in control of the positioning, emission rate, entanglement and quantum nonlinear generation by quantum emitters on silicon-based platforms.

I.1 Preservation of Quantum Coherence in Extremely Dispersive Media

Quantum plasmonics experiments have on multiple occasions reported the observation of quantum coherence of discrete plasmons, which exhibit remarkable preservation of quantum interference visibility, a seemingly surprising feature for systems mixing light and matter with high ohmic losses during propagation. However most experiments to date used essentially weakly-confined plasmons, which experience limited light-matter hybridization, thus limiting the potential for decoherence.

During the last year, we have observed quantum coherence of plasmons near the SPP resonance frequency, where plasmonic dispersion and confinement is much stronger than in previous

experiments. We generated polarization-entangled pairs of photons using spontaneous parametric down conversion and transmitted one of the photons through a plasmonic hole array designed to convert incident single photons into highly-dispersive single SPPs. We find the quality of photon entanglement after the plasmonic channel to be unperturbed by the introduction of a highly dispersive plasmonic element. Our findings provide a lower bound of 100 femtoseconds for the pure dephasing time for dispersive plasmons in gold, and show that even in a highly dispersive regime surface plasmons preserve quantum mechanical correlations, making possible harnessing the power of extreme light confinement for integrated quantum photonics.

I.2 Polarization Entanglement Measurements

Our approach utilized an experiment similar to that employed by Altewischer et al. (1). We generate pairs of polarization-entangled photons propagating along two different paths. We interpose a plasmonic hole array in the path of one of the photons. This photon is thus converted in a plasmon, and the detected signal consists of plasmons reconverted into free-space photons after plasmon propagation over a few hundred nanometers in the hole array. Whereas the work reported in (18) probed hole arrays with linear dispersion and circular holes, we investigate: i) first the influence of hole geometry the quality of entanglement in the linear regime and ii) second, we measure preservation of entanglement between photons when the plasmonic hole array operates in a highly dispersive regime, to probe plasmon decoherence.

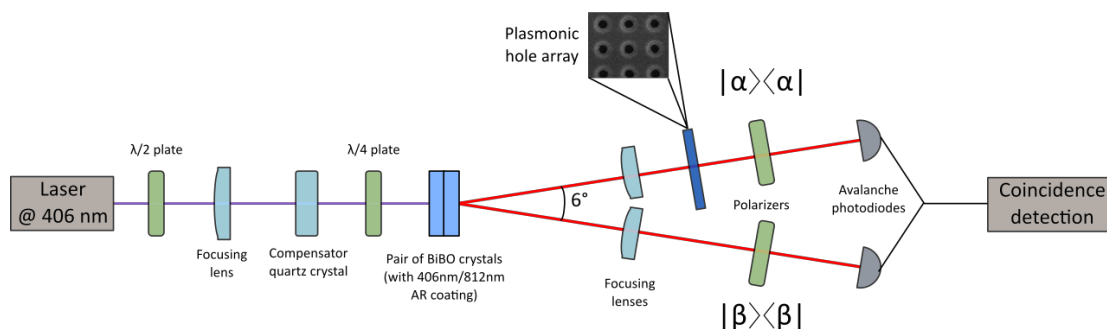


Figure 1. Experimental setup for the measurement of polarization-entanglement preservation. Pump photons at 406 nm are sent toward a pair of BBO crystals and generate pairs of polarization entangled photons that propagate along two separate paths. Along the upper path, we can insert a metallic hole array, and measure the transmission of the entangled light that has been coupled to plasmons.

Generation of entangled pairs of particles As a source of polarization-entangled photons we used type-I spontaneous parametric down-conversion (SPDC), occurring in a pair of nonlinear BiBO crystals. They are rotated by 90^0 with respect to each other and glued together (20) (Fig. 1), so that one crystal has its axis in the horizontal plane and the other one in a vertical plane. The pair of BiBO crystals is pumped by a laser diode emitting at 406 nm. The pump photons are linearly polarized at 45^0 with respect to the nonlinear crystal axis planes, so that type-I SPDC generate pairs of photons at 812 nm that are polarized parallel to either the horizontal direction or the vertical direction with equal probabilities. This setup generates polarization-entangled photons that, before their interaction with the environment $|E\rangle$ (plasmonic sample), can be described by the superposition state:

$$|\psi\rangle_{initial} = \frac{1}{\sqrt{2}} [e^{i\Delta\varphi_c} |H, H\rangle + |V, V\rangle] \otimes |E\rangle \quad (1)$$

where $\Delta\varphi_c$ is a phase delay between the two polarizations, due to the birefringence of BiBO crystals.

The twin photons propagate in a horizontal plane, along the opposite edges of a cone whose apex angle is 6° . Each photon is focused towards a polarizer and a single-photon avalanche diode (SPAD). The detection of a photon by one of the SPADs is a projective measurement of its polarization state. A plasmonic hole array can be placed along one of the propagation paths, thus forcing one of the photon to be temporarily converted into a plasmon before eventually being detected.

In our experiment, in order to correctly estimate the influence of pure dephasing processes, we retain only coincident counts between the two SPADs, i.e. we consider only the case when both photons register counts at the detectors. In other words, when the hole array is in place, we do not record events in which a plasmon has decayed through inelastic interactions with the electronic system – this is a well-understood mechanism for decoherence. On the contrary, we collect only photons from events in which the plasmon has survived. Such events, in principle, can be affected by elastic interactions or the inner structure of the plasmon quasiparticle.

In the general case, after propagation of the quantum entangled state and before applying any projective measurement, we can consider that the light has become entangled with the environment, and we can write

$$|\psi\rangle_{final} = \frac{1}{\sqrt{|h^2| + |v^2|}} [he^{i\Delta\varphi_c} |H, H\rangle \otimes |E_H\rangle + v|V, V\rangle \otimes |E_V\rangle]$$

where h and v – are complex amplitude transmission coefficients for horizontal polarization $|H\rangle$ and vertical polarizations $|V\rangle$ respectively; $|E_H\rangle$ and $|E_V\rangle$ are environmental states, entangled with horizontal and vertical polarizations respectively.

By tracing over environmental states one can obtain a reduced density matrix, from which a probability of a coincidence count can be computed:

$$\begin{aligned} P_{cc}(\alpha, \beta) &= \langle \alpha, \beta | \hat{\rho}_{reduced} | \alpha, \beta \rangle \\ &= \frac{1}{1 + \frac{|v^2|}{|h^2|}} \left[\sin^2 \alpha \sin^2 \beta + \frac{|v^2|}{|h^2|} \cos^2 \alpha \cos^2 \beta + \right. \\ &\quad \left. \frac{1}{2} \sin(2\alpha) \sin(2\beta) \frac{|v|}{|h|} |\langle E_V | E_H \rangle| \cos(\varphi_E + \Delta\varphi + \Delta\varphi_c) \right] \quad (3) \end{aligned}$$

where $\frac{v}{h} = \frac{|v|}{|h|} e^{-i\Delta\varphi}$, $\Delta\varphi$ being the phase difference between the complex amplitude h and v , $\langle E_V | E_H \rangle = |\langle E_V | E_H \rangle| e^{i\varphi_E}$, φ_E being the phase difference between the two environmental states, and α and β are the polarizer directions with respect to the vertical axis.

The first two terms can be obtained by classical analysis, whereas the last term is the so-called quantum interference term, which represents quantum mechanical nature of our system. Indeed, Eq. (2) describes a superposition state. The quantum interference term can be understood

as the interference amplitude between the two terms of the superposition state when projective measurements are carried out on the two-particle state. The amplitude of this term depends on several factors. It depends sinusoidally on the polarizers directions, and is maximum for appropriate choices of the polarizer directions verifying $|\sin(2\alpha) \sin(2\beta)| = 1$. This corresponds to the situation where the photonic parts of both terms in Eq. (2) are projected on a common state with equal amplitude. The amplitude of the quantum term is governed by the ratio $\frac{v}{h} = \frac{|v|}{|h|} e^{-i\Delta\varphi}$, which includes all perturbations inherent to the setup that affect the balance between the horizontal and the vertical polarization. Finally, we note here that the magnitude of quantum interference is also determined by the overlap between different environment states $\langle E_V | E_H \rangle = |\langle E_V | E_H \rangle| e^{i\varphi_E}$, which represents quantum mechanical decoherence. The presence of $\Delta\varphi_c$ in the last cosine factor of the quantum interference term shows that, in order to make judgements about quantum decoherence, one has to take a great care in eliminating or measuring phase differences between different polarizations. This can be done by inserting another birefringent element in the setup that will compensate the phase difference between the two polarizations. Optimization and alignment of our SPDC source included tweaking of a $\lambda/4$ plate (Fig. 1), which allowed us to experimentally eliminate $\Delta\varphi_c$ in equation (3).

Consider $h = v$, which represent equal probability of detecting horizontally or vertically polarized pairs of photons. In the case of absolute coherence $\langle E_V | E_H \rangle = 1$ ($E_V = E_H$) we get a rather simple expression $P_{cc}(\alpha, \beta) = \frac{1}{2} \cos^2(\alpha - \beta)$. There is no entanglement between the photon state and the environment. This ensures the preservation of polarization entanglement between photons. By contrast, in the case of total decoherence $\langle E_V | E_H \rangle = 0$ we get a straight line $P_{cc}(\alpha, \beta = 45^\circ) = \frac{1}{4}$ regardless of α (if β is kept fixed at 45°). Both terms of the superposition in (2) are now incoherent, and quantum interferences vanish. The measured state can be considered as a statistical mixture of the two states $|H, H\rangle$ and $|V, V\rangle$ in equal proportions.

These considerations suggest a measure of quality of the entanglement, visibility, which we define simply as the visibility of the cosine curve described by $P_{cc}(\alpha, \beta = 45^\circ)$ for the case when we keep polarizer β fixed at 45° (both polarizations contribute to the measurement) $V = \frac{P_{cc}^{max} - P_{cc}^{min}}{P_{cc}^{max} + P_{cc}^{min}}$, where P_{cc}^{min} is the minimum probability of coincidence count (rate in an experiment) and P_{cc}^{max} is the maximum rate. For $v = h$ the visibility is equal to $V = |\langle E_V | E_H \rangle| \cos(\varphi_E + \Delta\varphi + \Delta\varphi_c)$. From the above analysis we get that $V = 100\%$ for fully entangled (quantum) light ($\langle E_V | E_H \rangle = 1$), and $V = 0\%$ for a pure statistical mixture of polarizations (classical light, $\langle E_V | E_H \rangle = 0$). Note, that visibility of a cosine $P_{cc}(\alpha, \beta = 45^\circ)$ is identical to the visibility of the cosine $P_{cc}(\alpha, \beta = 135^\circ)$, hence we can use either one of them, or use one versus another to validate the correctness of the measurement.

In addition to that, we performed Bell's inequalities violation measurements, where we use Bell's inequalities in so-called CHSH form. We performed 16-point measurements in order to calculate Bell's parameter S , comparing our experimental measurement with the best possible prediction of any classical local hidden variable theory (LHVT). $S > 2$ indicates the impossibility of the explanation by any LHVT.

We characterized our SPDC source without plasmonic samples, measuring visibility on the order of $V = 99\% \pm 1\%$ and $S = 2.81 \pm 0.02$, which is just a standard deviation away from

the maximal theoretical value $S_{max} = 2\sqrt{2} \approx 2.83$. From this, we conclude that we have high quality pairs of entangled photons.

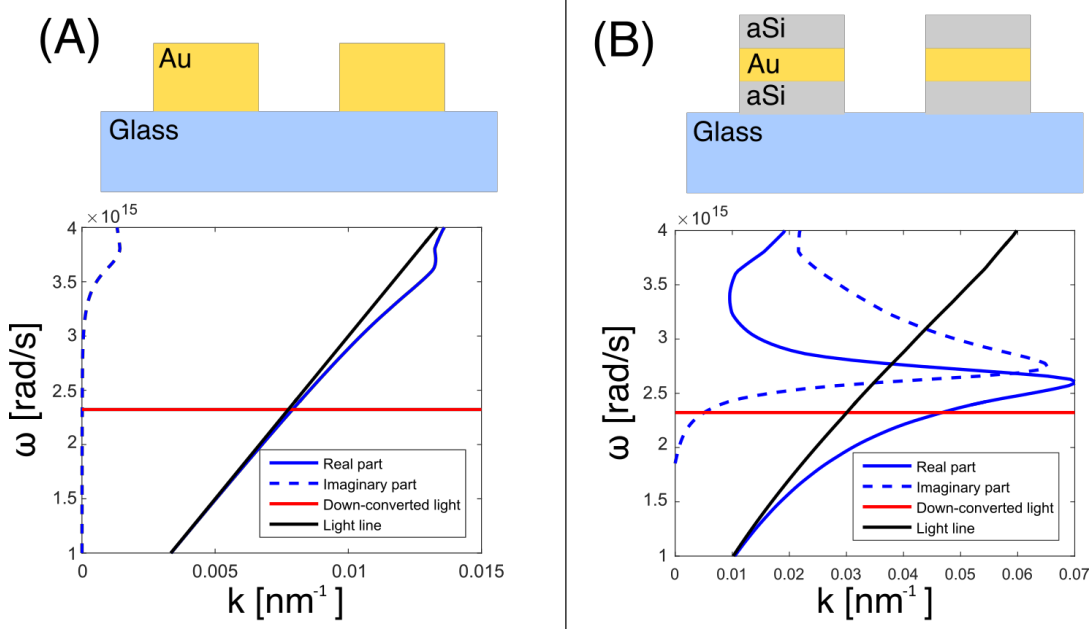


Figure 2. Plasmonic hole array design. (A) cross-sectional schematic and dispersion relation of elliptical hole arrays for SPPs supported at the gold/glass interface. At the wavelength of the down-converted photons (812 nm), the dispersion is ‘photon-like’, i.e., linear and very close to the light line; (B) cross-sectional schematic and dispersion relation of circular hole arrays for SPPs supported in the silicon/gold/silicon structure, which exhibits strongly nonlinear dispersion at 812 nm.

I.3. Hole arrays with nonlinear dispersion

We investigated polarization entanglement processes using single SPPs that propagate in a hole array with highly nonlinear dispersion, in an attempt to reveal effects of pure dephasing on decoherence through a decrease of entanglement visibility. We note that in the Born-Markov approximation, the visibility of entanglement is usually characterized by a decaying exponential $V \sim \exp\left(-\frac{t_p}{T_2^*}\right)$ where T_2^* is the pure dephasing time and t_p the propagation time of the plasmon.

In the highly dispersive regime, plasmons have a generally higher rate of interaction with the electronic system than in the case of materials with linear dispersion. Hence, in addition to shorter total decoherence time, one can expect a shorter pure dephasing time T_2^* (which is the relevant time scale probed by our experiment). On the other hand, the group velocity of highly dispersive plasmons is an order of magnitude smaller than for plasmons in the photon-like regime ($0.05c$ versus $0.59c$, where c is the speed of light in vacuum), so that these plasmons propagate for a longer time t_p (even if the propagation distances are the same). Therefore, for comparable experiments (i.e. similar propagation distances), strongly-confined plasmons are expected to experience greater decoherence and thus also exhibit weaker quantum interference than photon-like plasmons.

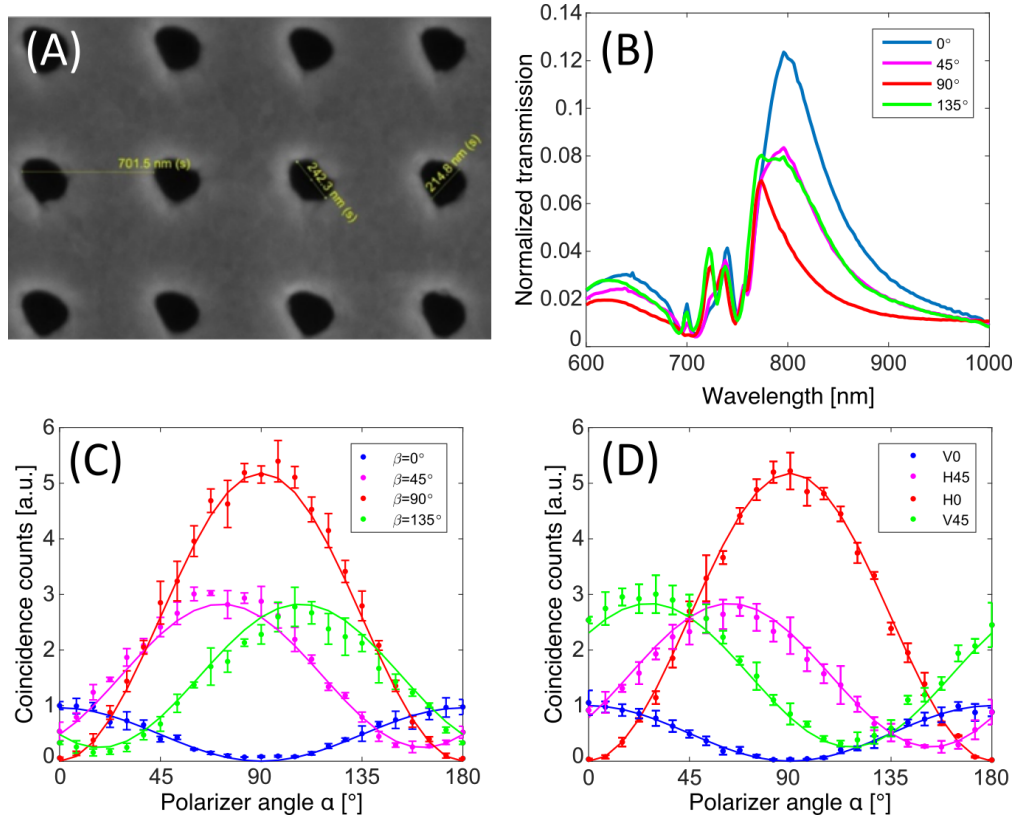


Figure 3. Entanglement preservation with the elliptical hole array. Elliptical hole array used to study the influence of hole geometry on the preservation of photon entanglement: **(A)** SEM image, where the orientation of the minor and major axis can be seen oriented at $\pm 45^\circ$; **(B)** transmission factor of the device for different polarizations of incident light. The holes do not have rotational symmetry, so that at 812 nm, transmission varies between 12.5 % for horizontally polarized light and 7% for vertically polarized light. **(C)&(D)** Normalized number of coincidence counts as a function of polarizer angles in the presence of an elliptical plasmonic hole array (solid line represents fit to the full model) in two configurations : **(C)** With entangled photons and for different fixed directions of the polarizer beta; **(D)** With classical light and similar choice for beta. The plots with $b=45^\circ$ and $b=135^\circ$ show a similar decrease in visibility in both configurations, indicating that this results from a purely classical effect.

In order to probe the highly dispersive regime, we used plasmons at the interface between gold and amorphous silicon. Amorphous silicon has a higher dielectric constant than air, moving the SPP resonance frequency close to the frequency of entangled photons (see Fig. 2(B)).

We used a 2mm by 2mm hole array configured in a three-layer structure (50nm of amorphous silicon – 100nm of gold – 50nm of amorphous silicon) and a periodicity $P=850\text{nm}$ (fig. 3(A)), following the same procedure of optimization as for the elliptical hole array. We find a plasmon-enhanced transmission peak at the desired 812nm wavelength (fig. 3(B)). In this hole array SPPs excited on the top and bottom gold surfaces are uncoupled and have the same dispersion.

Thanks to the larger size of the sample we were able to collect a larger portion of transmitted light and hence improve our statistics (fig. 3(C)). We recorded a visibility of $V = 98\% \pm 2\%$ and Bell's number $S = 2.83 \pm 0.04$: this measurement implies that even in the highly-dispersive regime, the entanglement is perfectly preserved and no quantitative signs of pure

dephasing could be detected. Through numerical computation of the dispersion relation, we can estimate the propagation time to be on the order of $t_p \sim \frac{1\mu m}{0.05c} \sim 70fs$ – much longer than the value of total dephasing time $T_2 = 2 T_1 = 20 fs$, that can be estimated from the absorption length in our sample (less than 200nm, in agreement with literature reported values (2)). Another approach towards an estimation of the propagation time based on an approximate Lorentzian fit of the resonance experienced by the plasmons gives a similar time. We therefore conclude that in our system, pure dephasing is a remarkably slow process compared to absorption, and the lower bound of the dephasing time can be estimated to be around 100 fs, which is similar to the value reported in (15). We note however that this time could be in practice much higher, as our experiment remarkably reports no quantitative trace of quantum decoherence, despite extreme plasmonic dispersion.

II.1 Dynamic Control of Quantum Dot LDOS and Purcell Enhancement of Spontaneous Emission by Electrical Gating of Plasmonic TiN

Emission control of colloidal quantum dots (QDs) foundational in modern high-quality lighting and display technologies. Dynamic emission control of colloidal QDs in an optoelectronic device is normally achieved by changing the optical pump intensity or injection current density. We have been investigating distinctly different mechanism for temporal modulation of QD emission intensity, at constant optical pumping rate. This mechanism is based on electrically controlled modulation of the local density of optical states (LDOS) at the position of QDs resulting in the modulation of the spontaneous emission rate, far-field emission intensity, and quantum yield of QDs. We can manipulate the LDOS via field effect-induced optical permittivity modulation of ultrathin degenerately doped titanium nitride (TiN) in a gated TiN/SiO₂/Ag plasmonic heterostructure. This demonstration of electrical control of the spontaneous emission rate for a visible-emitting fluorophore coupled to a plasmonic structure represents a new approach for intensity modulation in display and other optoelectronics applications.

Starting in mid-2016, we began investigating emission modulation of InP QDs embedded in the SiO₂ spacer layer of a TiN/SiO₂/Ag plasmonic heterostructure. The dependence of photoluminescence (PL) intensity on applied bias at the QD peak emission wavelength of $\lambda=630$ nm is shown in Fig. 4a. As one can see, the PL intensity monotonically increases with positive bias and monotonically decreases with negative bias. At $\lambda=630$ nm, the PL intensity change (normalized to the PL intensity at zero bias) is as high as 15% when gate voltage is varied between -1 V and $+1$ V. On the other hand, for QDs embedded in Ti/SiO₂/Ag passive heterostructure, no PL intensity modulation under applied bias is observed (Fig. 4b). Hence, at applied electric fields of 1.1 MV/cm, our InP/ZnS core-shell QDs show no quenching or red-shift of emission, which is characteristic for cadmium-based core-shell colloidal QDs. This is attributable to the large bandgap difference between InP core and ZnS shell materials. We also performed time-resolved PL measurements to identify the lifetime of QDs embedded in TiN/SiO₂/Ag heterostructures. When no electrical bias is applied, the measured lifetime of the InP QDs is 390 ps. At applied electrical bias of $+1$ V, the lifetime of QDs decreases by 12 %, while at the bias of -1 V, the lifetime increases by 18 % (Fig. 4c). Our calculations indicate that optical frequency electric field radiated by a QD is tightly confined in the SiO₂ layer and shows a considerable enhancement at the interface with TiN (Fig. 4d). As a result, the LDOS in the middle of SiO₂ layer is sensitive to modulation of the complex refractive index of TiN (Fig. 4d).

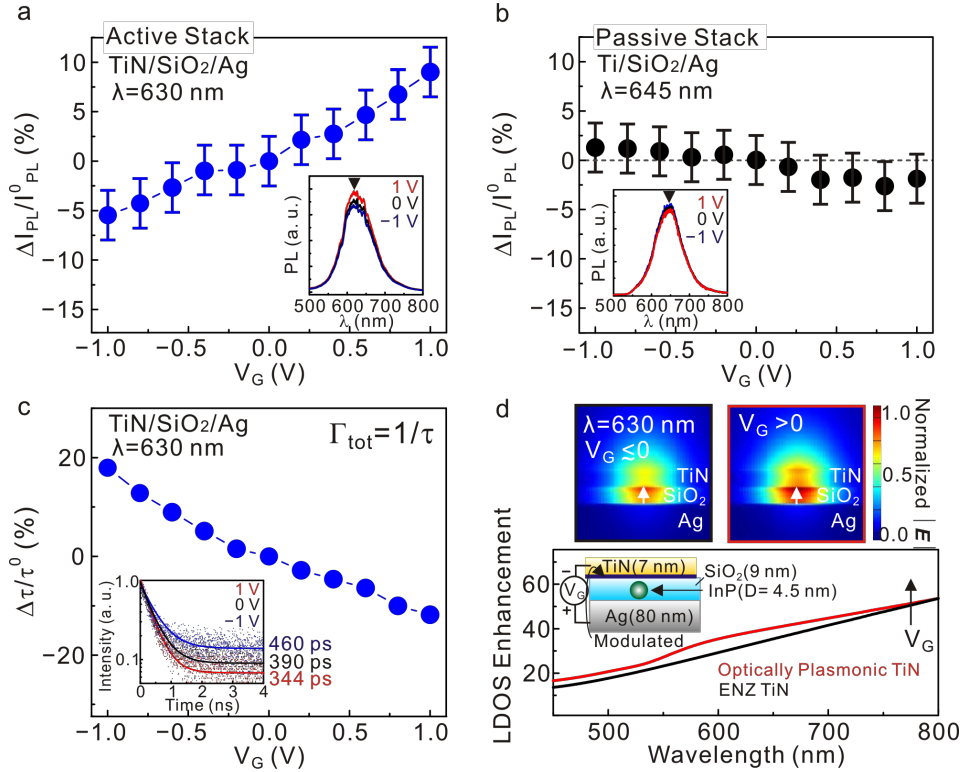


Figure 4. Gate-tunable spontaneous emission of QDs via modulation of the LDOS. In **a**, modulation of the PL intensity of InP/ZnS core-shell QDs embedded in the gated TiN/SiO₂/Ag plasmonic heterostructure (active stack) for wavelength of $\lambda=630$ nm. We observe a 10% PL relative intensity increase when the gate voltage V_G is varied from 0 V to +1 V. When V_G is varied from 0 V to -1 V we observe a 5% PL relative intensity decrease. The inset of **a** shows PL intensity spectra for different gate voltages. **b**, PL intensity of QDs embedded in gated Ti/SiO₂/Ag heterostructure (passive stack) for wavelength of $\lambda=630$ nm. No modulation of PL intensity is observed under an applied bias. The PL spectra for different gate voltages, plotted in the inset of **b**, also shows no modulation under applied bias. In **c**, PL lifetime of QDs embedded in the gated TiN/SiO₂/Ag plasmonic heterostructure. When the gate voltage V_G is increased from 0 V to +1 V, the QD lifetime decreases by 12%. When V_G is varied from 0 V to -1 V, the QD lifetime increases by 18%. The inset of **c** shows the PL intensity as a function of time for different gate voltages V_G . **d**, Calculated LDOS enhancement spectra at the position of QD for different carrier densities in a 1 nm thick modulated TiN layer. The black curve corresponds a homogeneous TiN film which is in the ENZ region ($n = 1.8 \times 10^{22} \text{ cm}^{-3}$). The red curve corresponds to a TiN film with a 1 nm thick modulated TiN layer that is plasmonic but far from the ENZ region). Top panels show the simulated spatial distribution of the optical frequency electric field $|E|$ radiated by a QD ($\lambda=630$ nm). Both the calculated LDOS and optical field intensity $|E|$ in the SiO₂ gap increase with gate voltage.

III. Si Chip-based Spontaneous Parametric Downconversion

1. General Theory for Spontaneous Parametric Downconversion in Complex Media

Single-photon and correlated two-photon sources are important elements for optical information systems. Nonlinear down-conversion light sources are robust and stable emitters of single photons and entangled photon pairs. However, the rate of downconverted light emission, dictated by the properties of low-symmetry nonlinear crystals, is typically very small, leading to

significant constraints in device design and integration. We developed principles of spontaneous emission control (i.e., the Purcell effect) generalized to describe the enhancement of nonlinear generation of quantum light through spontaneous parametric downconversion. We developed a theoretical framework based on eigenmode analysis to study quantum nonlinear emission in a general anisotropic, dispersive, and lossy media. Our theory provides an unprecedented insight into the emission process. We find that spontaneous parametric downconversion in a media with hyperbolic dispersion is broadband and phase-mismatch-free. We further predict a significant enhancement of the downconverted emission rate in experimentally realistic nanostructures. Our theoretical formalism and approach to Purcell enhancement of nonlinear optical processes provides a framework for description of quantum nonlinear optical phenomena in complex nanophotonic structures.

2. Chip-based GaP SPDC

In our proposal, we suggested using strained silicon with a silicon nitride overlay as the second order nonlinear material [3] for on-chip Si-based spontaneous parametric down conversion (SPDC). However, more recent research reports have cast doubt about the effectiveness of this material system for nonlinear applications [4]. Thus we took a different direction, focusing on GaP/Si integration. In our new design, gallium phosphide (GaP) was chosen as the nonlinear material because of its many attractive properties, including a large second order nonlinearity, transparency at short wavelengths enabling downconversion to 1550 nm, and small lattice mismatch with silicon. We have designed structure for downconversion both into dielectric waveguide modes and surface plasmons (SP). We have also made progress in transferring thin GaP film on low index substrates, which is the most critical step for implementation of our designs.

1) *Design of waveguides for SPDC*: The power conversion efficiency of SPDC in nanophotonic waveguide is given by the following equation [3]

$$\eta = \frac{16hc\pi^2 d_{eff}^2}{\epsilon_0 n_{e,p} n_{e,s} n_{e,i} \lambda_s^4 \lambda_i} \sin^2\left(\frac{\Delta\beta L}{2}\right) L^2 \frac{\delta\lambda_s}{A_i} \quad (4)$$

where $n_{e,p}$, $n_{e,s}$ and $n_{e,i}$ are the effective mode indices for the pump, signal and idler photons, L is the waveguide length, A_i is the effective mode area and $\delta\lambda_s$ is the detection bandwidth, $\Delta\beta$ is the momentum mismatch between the pump and the down converted photons.

The high field confinement ability of surface plasmons can be used for both device miniaturization and enhancement of nonlinear optical effects. Plasmonic down conversion therefore, will be a significant step towards development of compact on-chip quantum information systems. However, there are a number of issues which need to be addressed before such a scheme can be realized. One difficulty is to find proper nonlinear medium for such a scheme. Although GaP and other III-V semiconductors including AlGaAs and InP have large second order nonlinearities, the only nonzero components of the nonlinear susceptibility components are d_{14} , d_{25} and d_{36} , which allows only type 1 and type 2 SPDC. Since in case of plasmonic down conversion, both pump and downconverted photons will have same polarization (type 0 SPDC), a material which with nonzero d_{11} susceptibility is required. Current designs of integrated optic SPDC schemes uses long interaction length to achieve high conversion efficiency. This requires strict phase matching ($\Delta\beta=0$ in equation 1) between pump and down converted photons, which is often achieved by properly choosing appropriate pump and down converted modes. Since in plasmonic downconversion both pump and down converted photons are surface plasmons, it will be more difficult to satisfy the phase matching condition. The length of the plasmonic guide must

be small, so that there is low probability of losing one photon of the entangled photon pair due to absorption in the plasmonic waveguide itself. Therefore, a plasmonic SPDC scheme needs to be very compact, capable of working even when the phase matching condition is not completely satisfied and supporting type 0 SPDC. In the following, we describe our recent design that address these issues.

Although the bulk III-V semiconductors has no nonzero d_{11} susceptibility, the symmetry breaking at the surface can lead to a very large value of d_{11} at the surface. This has been experimentally verified by a number of recent works for several materials, including GaP [6]. We propose to use the strong surface nonlinearity of GaP [6] to overcome these limitations. Figure 1(a) shows the schematic of the waveguide design. The waveguide is a hybrid plasmonic waveguide with a thin TiO_2 film sandwiched between metal and GaP. As Fig. 5(b) shows the normalized electric field intensity at both pump and down converted wavelength (775 nm and 1550 nm) is very strong at GaP surfaces. The nonzero components of dominant nonzero component of surface nonlinearity is d_{11} which allows down conversion between for TM polarized (electric field normal to GaP- TiO_2 interface) pump and probe at these two wavelengths.

Although strict phase matching is essential for efficient second order nonlinear conversion in long waveguides, nanostructured optical materials e.g. plasmonic nanoparticles and semiconductor nanowires are capable of supporting these processes even when this condition is not satisfied [7]. The same would be true if we keep the length of the plasmonic guide short. To illustrate this, we have plotted the term $(\text{sinc}(\Delta\beta L)/2)^2$ from equation (4) in Fig. 5(c). This term represents the effect of phase mismatch on SPDC efficiency. The conversion efficiency is not significantly affected by phase mismatch, if the length of the plasmonic waveguide is restricted to few hundred nanometers. Keeping the plasmonic waveguide short will also minimize the effect of propagation loss on down converted photon, and both down converted photons should be able to emerge out of the plasmonic guide before being absorbed by the waveguide propagation loss. However, as we can see from Eq. (4), the conversion efficiency scales with square of waveguide length and restricting the waveguide length will limit the overall conversion efficiency. To overcome this, we propose to use the plasmonic slab waveguide geometry shown in Fig. 5(d). This will allow very efficient coupling of a large optical beam having large number of photons with the plasmonic waveguide and ensure high entangled photon generation rate.

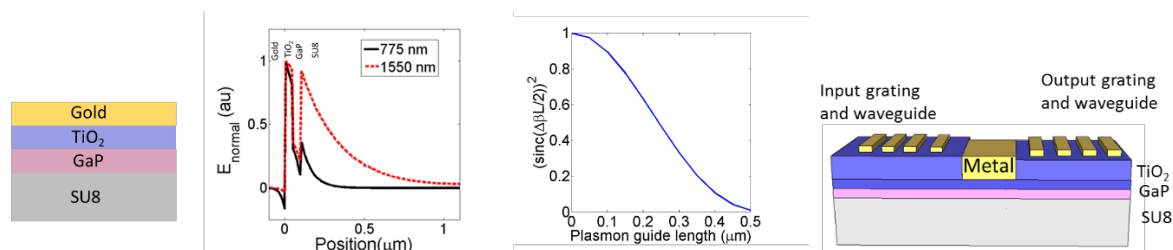


Figure 5 In (a), Hybrid plasmonic guide for SP to SP down conversion (b) Electric field profile normal to the interfaces for both pump and down converted modes (c) Effect of phase mismatch for various waveguide length (d) Proposed structure for plasmonic down conversion experiment.

In addition to plasmonic waveguide design we have also designed dielectric waveguide based down conversion scheme compatible with silicon photonics shown in Fig. 6. This design utilizes the bulk nonlinearity of GaP and the waveguide dimensions are chosen properly for achieving proper mode matching. We also have designed dielectric waveguide scheme capable of supporting type 0 SPDC, which was described in our previous report.

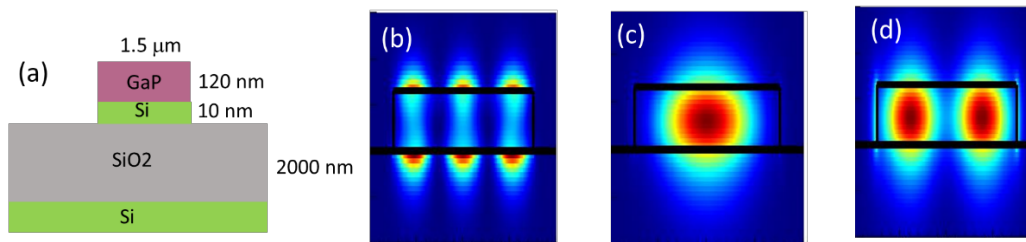


Figure 6. In, (a) Schematic of the nonlinear dielectric waveguide for SPDC. Electric field profiles for (b) Pump mode at 775 nm (c) and (d) Down converted mode at 1550 nm.

3. GaP thin film growth and transfer:

We have explored the feasibility of two different options to fabrication of single-crystal thin GaP films: transferring GaP from a silicon wafer to a glass substrate with an SU8 bonding layer, and MOCVD epitaxial growth of GaP on SOI wafers. In last 6 months we have focused more on the first approach. Figure 7(a) shows the configuration of a 50 nm thick GaP film initially grown on silicon which is bonded to SU8, and subsequently the silicon substrate is removed using XeF₂ etching. In our previous report, we described some progress in achieving continuous films with this approach. We have continued our work in optimizing this process, and have recently been able to achieve very smooth and continuous GaP film with only few defects over a large area, as shown in 7(b). The X-ray diffraction image of Fig. 7(c) confirms that the transferred material is indeed unstrained single-crystal (001)GaP.

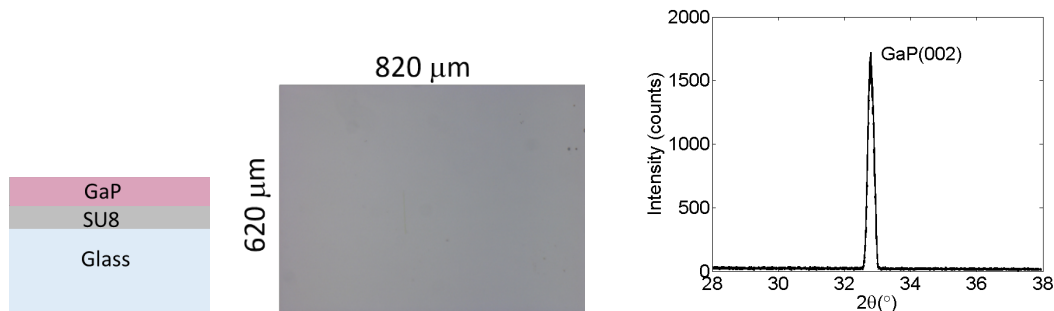


Figure 7(a) 50 nm GaP film transferred on SU8 (b) Optical image and of transferred film (c) X-Ray diffraction data showing GaP peak.

IV. Quantum Emitter Position and Orientation Control using DNA Origami Placement

The precise nanoscale control of both the positions and orientations of quantum emitters is a grand challenge for quantum nanophotonics. While previous methods have enabled either orientation or spatial position in the plane to be controlled for quantum dot, atomic or molecular quantum emitters, no general method for accomplishing *both* position and orientation control has been demonstrated to date. The inability to do this is currently a serious obstacle to building scalable systems composed of many quantum emitters. DNA origami placement (DOP) (8-10) is a potential solution to both challenges. We have been working over the last year in a collaboration with Dr. Paul Rothmund to develop a DNA origami technology capable of positioning and orienting quantum emitters. In DOP, the match between the overall shape of an origami and lithographically patterned binding sites is used both to position the origami in x and y, and to control its in-plane rotation angle. The strength of DOP is that thousands of origami can be oriented

with high yield and fidelity: $\sim 95\%$ of sites have single origami aligned within $\pm 10^\circ$ of a desired angle. Fig. 8(b)) results in a strongly anisotropic net dipole strength in the plane of the origami. Consequently, emission peaks for β perpendicular to the helix axes, coincident with θ . The strength of a molecular dipole μ excited by an electric field E along the direction of unit vector $\hat{e} = E/|E|$ is

$$D(E) = |\mu \cdot \hat{e}|^2 = |\mu|^2 \cos^2(\beta - \theta)$$

where β is the polarization of E , and the in-plane dipole angle. In the dipole approximation, emission is proportional to absorption, which is proportional to $|E|^2 D(E)$. This ability to position emitters should enable us to construct emitter arrays designed to test the superradiance properties of a finite number of emitters, and to construct subradiant ‘dark’ modes with engineering precision. A paper focusing on the emitter positioning and orientation distribution is currently in review at Science.

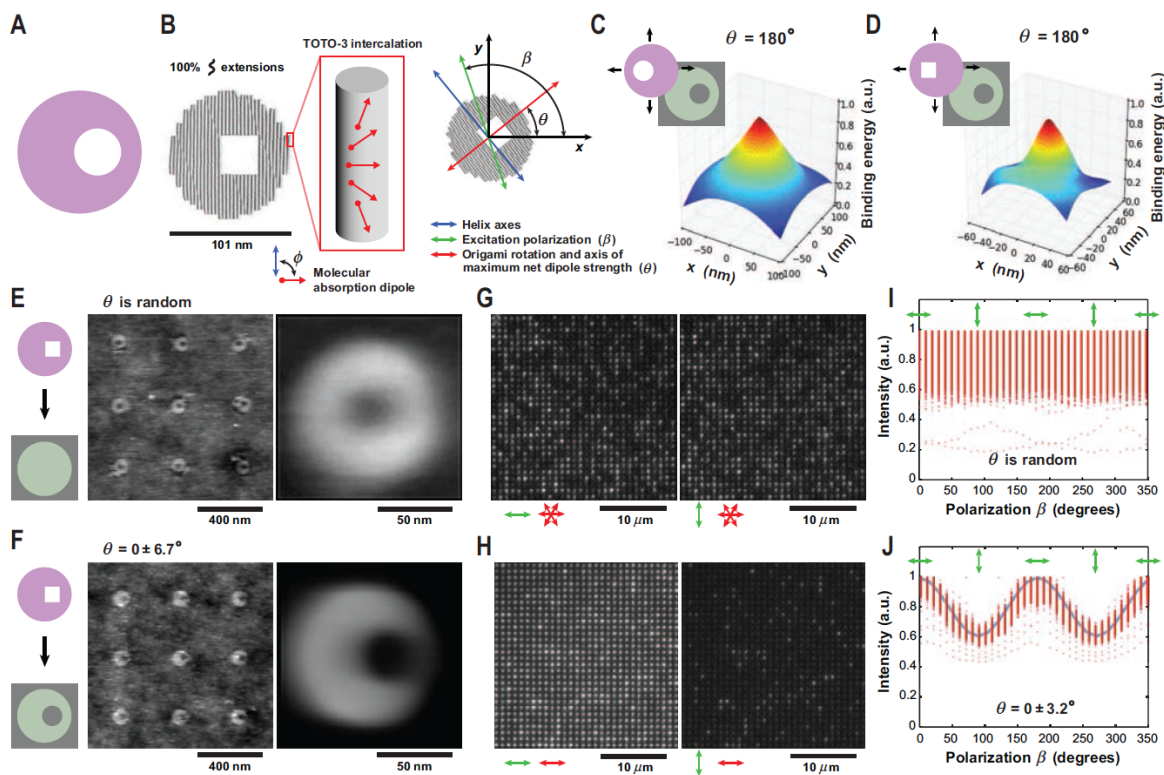


Figure 8. Breaking rotational symmetry. (A) Ideal ring with offset hole. (B) DNA origami approximation of (A) comprised of 34 parallel helix axes (gray cylinders). Inset shows rotation of the fluorescent dye TOTO-3’s absorption dipole along the length of a TOTO-3 intercalated helix. Coordinate system shows relationships between helix axes, excitation polarization (β) and origami rotation (θ). (C) Section of energy landscape for ideal shape (A) on binding site, $\theta = 180^\circ$. Colors run from high binding energy (red) to low (blue). (D) Same as (C), for experimental shape (B). (E and F) AFM and averaged AFM ($N=600$) of DOP on arrays of disk-shaped and shape-matched sites. (G and H) Fluorescence microscopy of TOTO-3 intercalated into DOP arrays on disk-shaped and shape-matched sites (ex. 642 nm; em. 660 nm). (I and J) Intensity (red dots) of $N=600$ sites in (G) and (H) as a function of excitation polarization. Blue line, best fit.

References:

- 1) E. Altewischer, M. P. van Exter, J. P. Woerdman, Plasmon-Assisted Transmission of Entangled Photons. *Nature* **418**, 304-306 (2002).
- 2) K. Puech, F. Z. Henari, W. J. Blau, D. Duff, G. Schmid, Investigation of the ultrafast dephasing time of gold nanoparticles using incoherent light. *Chemical Physics Letters* **247**, 13-17 (1995).
- 3) M. Cazzanelli et al. *Nature Materials* **11**: 148 – 154 (2012).
- 4) S. S. Azadeh et al. *Opt. Lett.* **40**: 1877-1880 (2015).
- 5) S. M. Spillane et al. *Optics Express* **15**:8770 - 8780 (2007)
- 6) R. Sanatinia, S. Anand, and M. Swillo, *Opt. Expr.* **23**: 756-764 (2015).
- 7) S. Liu et al. *Nano Letters* **16**: 5426 – 5432 (2016).
- 8) R. J. Kershner, L. D. Bozano, C. M. Micheel, A. M. Hung, A. R. Fornof, et al., *Nat. Nanotechnol.*, **4**(9):557–561,2009.
- 9) Erika Penzo, Risheng Wang, Matteo Palma, and Shalom J. Wind, *J. Vac. Sci. Technol. B*, **29**(6):06F205, 2011.
- 10) A. Gopinath and P. W. K. Rothmund, *ACS Nano*, **8**(12):12030–12040, 2014.

Personnel:

1. Yury Tokpanov, Graduate student, Applied Physics
2. Anya Mitskovets, Graduate student, Applied Physics
3. James Fakonas, Graduate student, Applied Physics
4. Yu Jung Lu, postdoc, Applied Physics
5. Artur R. Davoyan, postdoc Applied Physics

Awards to PI during grant period:

1. Elected Member, U.S. National Academy of Engineering, 2015
2. ISI Highly Cited Researcher 2015-2018
3. Member, National Academy of Inventors, 2016
4. David Adler Lectureship for Innovation in Materials Physics, American Physical Society 2016
5. American Physical Society Fellow, 2016
6. Kavli Innovations in Chemistry Lecture Award, American Chemical Society, 2018
7. Van Horn Distinguished Lecturer, Case Western Reserve University, 2018

Publications:

1. ‘Tunable Optical Response and Purcell Enhancement of Gated Plasmonic Structures’, Sokhoyan, R, Shirmanesh, GK, Lu, YJ, Thyagarajan, K, Pala, RA, Atwater, HA, 2017 International Conference on Optical MEMS and Nanophotonics, IEEE, Pages: 29-30 (2017).
2. ‘Dynamically controlled Purcell enhancement of visible spontaneous emission in a gated plasmonic heterostructure’, Lu, YJ, Sokhoyan, R, Cheng, WH, Shirmanesh, GK, Davoyan, AR, Pala, RA, Thyagarajan, K, Atwater, HA, *Nature Communications*, **8**, Article Number: 1631, DOI: 10.1038/s41467-017-01870-0 (2017).
3. ‘Dual-Gated Active Metasurface at 1550 nm with Wide (> 300 degrees) Phase Tunability’, Shirmanesh, GK (Shirmanesh, Sokhoyan, R, Pala, RA, Atwater, HA, *Nano Letters*, **18** Pages: 2957-2963, DOI: 10.1021/acs.nanolett.8b00351 (2018).
4. ‘Quantum nonlinear light emission in metamaterials: broadband Purcell enhancement of parametric downconversion’, Davoyan, A, Atwater, H, *Optica*, **5** Pages: 608-611, DOI: 10.1364/OPTICA.5.000608 (2018).
5. ‘Optical magnetism in planar metamaterial heterostructures’, Papadakis, GT, Fleischman, D, Davoyan, A, Yeh, P, Atwater, HA, *Nature Communications*, **9**, Article Number: 296, DOI: 10.1038/s41467-017-02589-8 (2018).
6. ‘Quantifying the role of surface plasmon excitation and hot carrier transport in plasmonic devices’, Tagliabue, G, Jermyn, AS, Sundararaman, R, Welch, AJ, DuChene, JS, Pala, R, Davoyan, AR, Narang, P, Atwater, HA, *Nature Communications*, **9**, Article Number: 3394, DOI: 10.1038/s41467-018-05968-x (2018).

7. ‘Subwavelength integrated photonics’, Cheben, P., Halir, R., Schmid, JH., Atwater, HA, and Smith, DR , *Nature*, **560** Pages: 565-572, DOI: 10.1038/s41586-018-0421-7 (2018).
8. ‘Modulated Resonant Transmission of Graphene Plasmons Across a $\lambda/50$ Plasmonic Waveguide Gap’, Jang, MS, Kim, S, Brar, VW, Menabde, SG, Atwater, HA, *Physical Review Applied*, **10**, Article Number: 054053 DOI: 10.1103/PhysRevApplied.10.054053 (2018).
9. ‘Mimicking surface polaritons for unpolarized light with high-permittivity materials’, Papadakis, GT., Davoyan, A, Yeh, P, and Atwater, HA, *Physical Review Materials* **3**, Article Number: 015202; Accepted October 2018; Published: Jan 10 2019.
10. ‘Quantum Coherence is Preserved in Extremely Dispersive Plasmonic Media’, Yury S. Tokpanov, James S. Fakonas, Benjamin Vest, Harry A. Atwater, arXiv:1810.00114, quant-ph cond-mat.mes-hall physics.app-ph
11. ‘Absolute and arbitrary orientation of single molecule shapes’, Ashwin Gopinath, Chris Thachuk, Anya Mitskovets, Harry A. Atwater, David Kirkpatrick, Paul W. K. Rothmund, arXiv:1808.04544 [pdf, other] physics.app-ph cond-mat.mes-hall cond-mat.soft physics.atm-clus physics.bio-ph (*Science*, in press).

Patents:

1. Optical Modulating Device Having Gate Structure, Atwater, Harry A, Sokhoyan, Ruzan, Kafaie Shirmanesh, Ghazaleh, Han, Seunghoon, Lu, Yu-Jung, Pala, Ragip A, Lee, Ho Wai, Huang, Yao-Wei, Thyagarajan, Krishnan, filed 7/20/2016, patent number 10,012,852, (filed in US and Korea).